Metabolite sequestration enables rapid recovery from nutrient depletion

Christopher Hartline[1,†], Ahmad A. Mannan[2,3†], Fuzhong Zhang[1,*], Diego A. Oyarzún[4,5,*]

[1] Department of Energy, Environmental & Chemical Engineering, Washington University in St Louis, St. Louis, 63130, USA

[2] Department of Mathematics, Imperial College London, London SW7 2AZ, UK

[3] Current address: School of Engineering, University of Warwick, Coventry CV4 7AL, UK

[4] School of Informatics, University of Edinburgh, Edinburgh EH8 9AB, UK

[5] School of Biological Sciences, University of Edinburgh, Edinburgh EH9 3BF, UK

[†] Equal contribution

[*] Corresponding authors: F. Zhang (fzhang@seas.wustl.edu) and D. A. Oyarzún (d.oyarzun@ed.ac.uk).

Microbes adapt their metabolism to take advantage of nutrients in their environment [1]. Upon changes in nutrient conditions, transcriptional programs adapt pathway expression to meet the cellular energy budget [2]. Since nutrient abundance may change frequently, rapid pathway recovery is just as important as fast activation. Yet little is known about the regulatory strategies that microbes employ to accelerate their recovery from nutrient depletion. Using the fatty acid catabolic pathway in *Escherichia coli* as a model system, we show that fast recovery can be achieved by rapid release of a transcriptional regulator from a metabolite-sequestered complex. With a combination of theory and experiment, we show that recovery dynamics depend critically on the rate of metabolite consumption and the duration of the exposure to nutrient. We constructed and compared strains with re-wired regulatory architectures, which highlight negative autoregulation as a superior control strategy over constitutive expression and positive autoregulation. Our results have wide-ranging implications for our understanding of metabolic homeostasis and the design of gene control circuits for synthetic biology and metabolic engineering.

Bacteria constantly adapt to changing environments by coordinating multiple levels of their intracellular machinery. The regulatory systems that enable rapid adaptations to nutritional changes require a complex interplay between metabolic genes and metabolites [3], which shapes cell fitness, bet hedging efficacy, population survival, as well as competition among microbiota.

Metabolite-gene interaction via metabolite-responsive transcription factors (MRTFs) is a common strategy that microbes employ to sense nutrient availability and to autonomously orchestrate changes in gene expression and metabolic flux [4]. Upon nutrient induction, cellular resources are invested in expressing enzymes dedicated to nutrient uptake. After nutrient depletion the uptake enzymes are no longer required, so control mechanisms down-regulate their expression to save cellular resources. While much of the literature has focused on the roles of MRTF control systems during nutrient induction [4, 5], there is little understanding of how these systems regulate recovery dynamics after nutrient depletion.

The MRTF-regulated nutrient induction is a balanced process between response kinetics and resource economy. Inducible expression systems are associated with a cost of having to synthesize the sensing component (e.g. MRTF). A rapid response to changing environments can achieve a higher cellular fitness, overcoming the invested cost of expressing the sensing component [6]. While typical inducible systems take a number of cell cycles for the expressed proteins to reach steady state [7], transcriptional regulation can affect the response time during

induction. For instance, negative autoregulation has been shown to speed up gene expression [4], and metabolic feedback circuits can accelerate metabolite response [8]. However, how the control system exploits both regulatory architecture and parameters to shape the recovery dynamics is not well understood. Cells that rapidly shut down their metabolic pathways during depletion can avoid waste of limited resources and potentially gain growth benefits.

In this paper, we study a regulatory architecture commonly found in bacterial metabolic systems [9] (Figure 1A and Table S1). In absence of nutrient, a MRTF represses expression of uptake and catabolic enzymes. When the nutrient becomes available, the internalized nutrient binds and sequesters the transcription factor, thus relieving the repression of metabolic enzymes and allowing nutrient import and utilization. In several instances of this control system, the transcription factor also represses its own expression (Table S1).

Using the *Escherichia coli* fatty acid catabolic pathway as a model system, we studied its dynamics in response to nutrient (oleic acid) shift between an ON- and OFF-state, defined as an environment with and without the presence of oleic acid (Figure 1B). In the ON-state, oleic acid is imported as fatty acyl-CoA by small amounts of the transporter FadD. As intracellular acyl-CoA accumulates, it binds to the transcription factor FadR and sequesters it into a complex. The sequestering unbinds FadR from DNA [10], which relieves the repression of FadD and accelerates oleic acid import, forming positive feedback loop. This allows a rapid transition to the ON-state [11]. After switching to the OFF-state, release of free FadR from the complex recovers its inhibition on the expression of unnecessary catabolic enzymes.

We built a kinetic model based on four core components of the regulatory system: FadD (*D*), free FadR (*R*), acyl-CoA (*A*) and sequestered FadR (a-R), and parameterized it using experimentally measured time course data after induction with various concentrations of oleic acid (details in Methods). From model simulations, we defined two metrics to quantify the recovery after the switch from ON- to OFF-state (Figure 1C). First, we define the recovery time (τ_{50}) as the time taken for FadD to decrease to half-way between its maximum and minimum steady state value after nutrient depletion (Figure 1C). Second, we defined the metric η as the proportion of free FadR released from the sequestered complex after one doubling time:

$$\eta = \frac{\mathrm{FadR_{DT}} - \mathrm{FadR_{DT-new}}}{\mathrm{FadR_{DT}}},$$

where $\mathrm{FadR_{DT}}$ and $\mathrm{FadR_{DT\text{-}new}}$ are the concentration of free FadR and the concentration of newly expressed FadR in the OFF-state after one doubling time. This definition allows us to quantify the contribution of free FadR released from the sequestered pool to the recovery dynamics. We simulated the pathway recovery kinetics during the OFF-state for varying concentrations of the acyl-CoA-consuming enzyme and the time spent in the ON state (t_0). These two parameters affect the amount of acyl-CoA available for sequestration and the amount of free FadR when the nutrient is depleted, respectively. Simulation results (Figure 2A) suggest that the recovery time shortens with the

concentration of consuming enzyme, while released FadR (η) increases with both the consuming enzyme and the time spent in the ON state. Further simulations suggest that when the ON-state is kept for longer time, the pool of acyl-CoA accumulates and takes a long time to be consumed in the OFF-state. This delays the release of FadR from the complex and results in a longer recovery time (details in Supplementary Information S3 and Figure S4). Model simulations also reveal a strong inverse relation between τ_{50} and η (Figure 2B), indicating that the release of FadR from sequestration by acyl-CoA provides a mechanism to achieve rapid recovery during nutrient depletion. The sensitivity of this inverse relation increases when cells are exposed to a longer ON-state, because this leads to larger pools of sequestered FadR.

To verify the model predictions, we sought to experimentally increase the fraction of released FadR (η) with two complementary strategies. We first decreased the rate of consumption of acyl-CoA by deleting the *fadE* gene, which encodes the second step of the fatty acid β-oxidation pathway. This prevents metabolization of acyl-CoA by β-oxidation, and leaves membrane incorporation (catalyzed by enzyme PlsB) as the only pathway for acyl-CoA consumption. We measured *fadD* expression dynamics after switching the strains from the ON-state (M9G + 1mM oleic acid media) to OFF-state (M9G media) using a red fluorescent protein (RFP) reporter fused downstream of the *fadD* promoter. In agreement with model predictions (Figure 2C), the *fadE* knockout strain displayed a slower recovery than the wild type, with ~60% increase in recovery time (Figure 2D). This entails an increased expenditure of biosynthetic resources to import a metabolite that is no longer present in the environment.

Next, we measured the *fadD* recovery dynamics after switching the cultures from growth in the ON-state for t_0= 3, 6, and 9 hours (Figure 1C). The resulting recovery times displayed a good qualitative agreement with model simulations (Figures 2E,F). Recovery time did not show significant differences between 6 and 9 hours, possibly because slower recovery is counteracted by the delay of having to consume a higher level of accumulated acyl-CoA, or because the maximum level of sequestered FadR may already have been achieved at 6 hours.

Among the uptake systems in *E. coli* with the architecture of Figure 1A, we found that the majority have a transcriptional regulator that represses its own expression, few have constitutive expression of the regulator, and none display positive autoregulation (see Table S1). To better understand the salient features of each regulatory architecture and how they affect recovery dynamics, we built variants of our kinetic model with FadR under constitutive expression and positive or negative autoregulation (details in Methods). Simulations of the switch from the ON- to OFF-state suggest that these architectures behave similarly for short times spent in the ON-state, quickly sequestering all the free FadR (Figure 3A). But for longer times in the ON-state, we found important differences in the dynamics of the level of sequestered FadR between the various modes of autoregulation. Negative autoregulation leads to large accumulation of sequestered FadR, while positive autoregulation leads to an overall depletion of sequestered FadR. Constitutive expression, on the contrary, enabled the total level of FadR,

primarily in the sequestered form, to be maintained at a constant level. Analysis of model equations reveals that these are structural properties of the model. We show mathematically (details in Supplementary Information S4) that after a long time in the ON-state, the steady state concentration of total FadR upon nutrient depletion follow the trends as we observed in Figure 3A (top), irrespective of model parameters. Simulations indicate that the overall relation between recovery time and induction time is similar across the three architectures (Figure 3A bottom inset). However, for positive autoregulation we found recovery to be significantly slower for a wide range of induction times. To test this prediction, we engineered an *E. coli* strain with positively autoregulated FadR expression by replacing the native *fadR* promoter with one that activated by FadR (P_{fadRpo}, see Supplementary information S8), and a P_{fadD} reporter plasmid. The positively autoregulated reporter strain (PA-reporter, Supplementary Table S5,6) was grown in the ON-state (M9G media + 1mM oleic acid) and then rapidly switched to the OFF-state (M9G media) after 3, 6 and 9 hours. We measured the *fadD* expression dynamics (Supplementary Information S8, Fig. S7), and calculated the respective recovery times (Figure 3B). Consistent with model predictions, recovery times for the positively autoregulated strain increased with the time spent in the ON-state.

Model analysis suggests that both constitutive expression and negative autoregulation can sequester high amounts of FadR for long times in the ON-state. We also found that for high concentrations of oleic acid, the steady state concentration of sequestered FadR in the ON-state scales linearly with *fadR* promoter strength (Supplementary Information S5). Simulations of both systems with increasing promoter strength reveal that increased FadR sequestration in the ON-state cause a decrease in recovery times (Figure 4A). The results moreover suggest that *fadR* promoter strength can be tuned to achieve the same recovery time in both regulatory architectures.

Since release of sequestered FadR has a direct impact on recovery time, we sought to identify the benefits that make negative autoregulation favored over constitutive expression. Since production of FadR entails a biosynthetic cost, we compared both regulatory architectures in terms of the cost of FadR synthesis. From time-course simulations for varying fadR promoter strengths (Figure 4B), we computed the total amount of synthesized FadR in the ON- and OFF-states. Results suggest that both architectures require identical biosynthetic costs in the ON-state, but negative autoregulation leads to significant savings in the OFF-state (Figure 4C) as compared to constitutive expression. Therefore, although both architectures can in principle achieve the same recovery time, negative autoregulation achieves this with a lower cost on synthesis of the transcription factor.

Overall, we find that rapid release of free FadR from acyl-CoA sequestered a-R complex shortens the recovery time. Our simulations and experiments have shown that increasing the amount of stored FadR during induction and increasing consumption of the sequestering metabolite (acyl-CoA) expedites free FadR releasing, thus shortening the recovery time. Through our model simulations, we observed a delayed recovery driven by the need

to reduced metabolite concentration to levels required to release free TF from stored complex. During the delay, wasteful expression of the uptake pathway was continued despite the absence of nutrient. Previous research has shown that upon induction, metabolite dynamics tend to lag behind slow production of metabolic enzymes [8]. Interestingly, here we find that after inducer depletion, the recovery of protein production can be limited by the metabolite dynamics. This has important implications for designing synthetic control circuits that utilize non-metabolizable inducers, such as IPTG. With no consumption of the inducer, post-induction recovery response will be slow and cause a dramatic drain of cellular resources.

Further theoretical analysis revealed principles that explain how autoregulation shapes the recovery time. We found that negative autoregulation of the transcription factor provides a resource-saving strategy for the recovery dynamics. We found that MRTFs in 13 out of 18 nutrient uptake systems (see Table SF1) have negative autoregulation, suggesting an evolutionary pressure for a resource-saving control strategy. Past studies in the literature have found that expression under negative autoregulation can decrease response times in gene expression [7], linearize dose-response in responsive systems [12], and even speed up metabolic dynamics [8]. In addition to these properties, we find that negative autoregulation enables faster and more resource-saving metabolic recovery to nutrient depletion.

Recent efforts in synthetic biology focus on engineering gene control circuits to manipulate microbial metabolism. In large fermentations, microbial hosts face highly heterogeneous and dynamic environments. Our results provide core design principles for synthetic gene circuits. These design rules can help to achieve rapid recovery and to mitigate against deleterious nutrient fluctuations, and are useful in applications at the interface of synthetic biology and metabolic engineering.

References

1. Chubukov, V., et al., *Coordination of microbial metabolism.* Nat Rev Microbiol, 2014. **12**(5): p. 327-40.
2. Weisse, A.Y., et al., *Mechanistic links between cellular trade-offs, gene expression, and growth.* Proc Natl Acad Sci U S A, 2015. **112**(9): p. E1038-47.
3. Piazza, I., et al., *A Map of Protein-Metabolite Interactions Reveals Principles of Chemical Communication.* Cell, 2018. **172**(1-2): p. 358-372 e23.
4. Kotte, O., J.B. Zaugg, and M. Heinemann, *Bacterial adaptation through distributed sensing of metabolic fluxes.* Mol. Syst. Biol., 2010. **6**: p. 355.
5. Bettenbrock, K., et al., *A quantitative approach to catabolite repression in Escherichia coli.* J. Biol. Chem., 2006. **281**(5): p. 2578-2584.
6. Geisel, N., *Constitutive versus responsive gene expression strategies for growth in changing environments.* PLoS One, 2011. **6**(11): p. e27033.
7. Rosenfeld, N., M.B. Elowitz, and U. Alon, *Negative autoregulation speeds the response times of transcription networks.* J. Mol. Biol., 2002. **323**(5): p. 785-793.
8. Liu, D. and F. Zhang, *Metabolic Feedback Circuits Provide Rapid Control of Metabolite Dynamics.* ACS Synth. Biol., 2018. **7**(2): p. 347-356.

9. Keseler, I.M., et al., *The EcoCyc database: reflecting new knowledge about Escherichia coli K-12.* Nucleic Acids Res., 2017. **45**(D1): p. D543-D550.
10. Cronan, J.E., Jr., *In vivo evidence that acyl coenzyme A regulates DNA binding by the Escherichia coli FadR global transcription factor.* J Bacteriol, 1997. **179**(5): p. 1819-23.
11. Alon, U., *Network motifs: theory and experimental approaches.* Nat. Rev. Genet., 2007. **8**(6): p. 450-461.
12. Madar, D., et al., *Negative auto-regulation increases the input dynamic-range of the arabinose system of Escherichia coli.* BMC Syst. Biol., 2011. **5**: p. 111.
13. Lee, T.S., et al., *BglBrick vectors and datasheets: A synthetic biology platform for gene expression.* J. Biol. Eng., 2011. **5**: p. 12.
14. Engler, C., R. Kandzia, and S. Marillonnet, *A one pot, one step, precision cloning method with high throughput capability.* PLoS One, 2008. **3**(11): p. e3647.
15. Jiang, Y., et al., *Multigene editing in the Escherichia coli genome via the CRISPR-Cas9 system.* Appl. Environ. Microbiol., 2015. **81**(7): p. 2506-2514.
16. Liu, D., et al., *Negative feedback regulation of fatty acid production based on a malonyl-CoA sensor-actuator.* ACS Synth. Biol., 2015. **4**(2): p. 132-140.
17. van Aalten, D.M., et al., *Crystal structure of FadR, a fatty acid-responsive transcription factor with a novel acyl coenzyme A-binding fold.* EMBO J., 2000. **19**(19): p. 5167-5177.

Materials and Methods

Materials. Phusion DNA polymerase, T4 DNA ligase, restriction enzymes, and Teknova 5x M9 minimal salts were purchased from Thermo Fisher Scientific (Waltham, MA, USA). Gel purification and plasmid miniprep kits were purchased from iNtRON Biotechnology (Lynnwood, WA, USA.). Oligonucleotides were synthesized by Integrated DNA Technologies (Coralville, IA, USA). All other reagents were purchased from Sigma-Aldrich (St. Louis, MO, USA.)

Plasmids, strains, and genome modifications. A list of plasmids used along with promoter sequences in this study is provided in Supplementary Information S7 (Tables S4 and S5). *E. coli* DH10β was used for plasmid construction. The plasmid pSfadDk-rfp was constructed by cloning the *fadD* promoter (500 bp upstream of its translation start site) into the 5' of a *rfp* gene in a BglBrick vector, pBbSk-rfp [13] using Golden Gate DNA Assembly [14]. The positively autoregulated *fadR* strain was engineered by replacing *fadR*'s native promoter with a FadR-activated promoter P_{fadRpo} via CRISPR-Cas9 genome editing [15]. Detailed engineering methods and the characterization of the P_{fadRpo} promoter are described in Supplementary Information S8.

Three reporter strains were created to measure expression kinetics from the *fadD* promoter. These strains were created by transforming plasmid pSfadDk-rfp into either the wild-type DH1 strain, DH1(ΔfadE), or an engineered strain with positively autoregulated *fadR*, resulting in WT-reporter, ΔfadE-reporter, and PA-reporter, respectively.

Media conditions. All strains were grown from single colonies and cultivated overnight in Luria-Bertani (LB) media before experiments. For OFF-State culture conditions, cells were grown in M9 minimal media [16] supplemented with 1% glycerol and 0.5% Tergitol Solution Type NP-40 (M9G). For ON-state culture conditions, cells were grown

in M9G + 1 mM oleic acid (M9G+OA). All cultures were supplemented with appropriate antibiotic selection (50 mg/L Kanamycin, 100 mg/L Ampicillin).

Assays of fadD expression kinetics. To measure the recovery dynamics, reporter strains were grown in 3 mL M9G+OA for 24-48 hours at exponential growing state. To rapidly switch nutrient, cells were centrifuged (5500 rcf, 2 minutes) and washed twice in M9G. Cultures were then diluted in M9G medium to OD_{600} = 0.08 and transferred to a Falcon 96-Well Imaging Microplate (Corning, NY, USA). The microplate was then incubated in an Infinite F200PRO plate reader (TECAN, Männedorf, Switzerland) at 37°C with constant shaking. To maintain exponential growth during measurement, cultures were diluted by a factor of 5 for three times during incubation. Kinetic measurements of cell density (absorbance at 600 nm) and RFP fluorescence (excitation: 584 ± 9 nm, emission: 620 ± 20 nm) were taken every 900 seconds until all diluted cultures reached stationary phase. Fluorescence from water in the same 96-well plate was used as the background and was subtracted from all fluorescence measurements. The background-corrected fluorescence was later normalized by cell density. To calculate the recovery time, the average of three biological replicates were fitted to an exponential curve:

$$F = a \times e^{-b*t} + c$$

where *F* is the background-corrected, cell-density-normalized fluorescence. The recovery time was calculated as $\tau_{50}=\log(2)/b$.

For switches after defined times in the ON-state, cultures were first grown in exponential growth phase for 24-28 hours in M9G. Samples from these cultures were then centrifuged (5500 rcf, 2 minutes) and suspended in M9G+OA with an initial OD_{600} of 0.08 and cultivated in 96-well plates for various amount of time as indicated.

Kinetic model of fatty acid uptake. To study the system dynamic response to induction (ON-state) and its post-induction recovery (OFF-state) (Fig. 1C), we built a kinetic model for fatty acid uptake. We define the kinetic model as a system of ODEs describing the rate of change of each system component:

$$\frac{dR}{dt} = P_R(R, p_r) - k_f \cdot R \cdot A^2 + k_r \cdot \mathrm{aR} - \mu \cdot R, \quad (6)$$

$$\frac{dD}{dt} = b_D + \frac{a_D}{1+(K_D \cdot R)^2} - \mu \cdot D, \quad (7)$$

$$\frac{dA}{dt} = \frac{k_{cat,D} \cdot \mathrm{OA}}{K_{m,D}+\mathrm{OA}} \cdot D - \frac{k_{cat,B} \cdot A}{K_{m,B}+A} \cdot B - 2 \cdot (k_f \cdot R \cdot A^2 - k_r \cdot \mathrm{aR}) - \mu \cdot A, \quad (8)$$

$$\frac{d\,\mathrm{aR}}{dt} = k_f \cdot R \cdot A^2 - k_r \cdot \mathrm{aR} - \mu \cdot \mathrm{aR}, \quad (9)$$

where *R*, *D*, *A* and aR represent the concentrations of transcription factor FadR, uptake enzyme FadD, internalized fatty acid acyl-CoA, and sequestered complex acyl-CoA-FadR, respectively (Fig.1B). The reversible sequestering of one FadR dimer by two acyl-CoA molecules (stoichiometry as defined in [17]) is modeled as mass-action kinetics in

the term $k_f RA^2 - k_r \mathrm{aR}$. The term $P_R(R, p_r)$ represents the expression and autoregulation of the fadR promoter. To model FadR negative autoregulation for the wild-type strain, we use

$$P_{R,n} = b_n + \frac{a_n}{1+K_n \cdot R}. \quad (10)$$

Further details of the model are given in Supplementary Information S2, and descriptions of parameters in Table S2. We parameterized the model with time course data of RFP expressed from a *fadD* promoter induced at different oleic acid concentrations, and fitted values can be found in Table S3. Details of the experimental strain, the data used and the fitting process are given in Supplementary Information S2. For the models with constitutive expression and positive autoregulation of FadR, we use

$$P_{R,p} = b_p + \frac{a_p \cdot K_p \cdot R}{1+K_p \cdot R}, \quad (2)$$

$$P_{R,c} = p_c. \quad (3)$$

Model simulations. The kinetic model of the fatty acid uptake control system (Fig. 1A) was solved in MATLAB R2018a, using the ODE solver suite. To simulate the ON-state, simulations were initialized using the steady state values achieved from running simulations in absence of oleic acid (OA = 0 µM). A constant level of oleic acid was set at t = 0, with OA = 1000 µM in Eq.(8), and simulations were run to steady state, or a defined time (to emulate time spent in ON-state). To simulate the OFF-state, the system was initialized using either the steady state or end-point values achieved in the ON-state, but now with OA = 0 µM in Eq.(8). Simulations of the OFF-state were run to steady state, and recovery times were calculated from a measure of the time from the start of the OFF-state till when FadD reached half-way between its initial (max) value and minimum steady state value.
In Figure 3, for fair comparison model parameters are set such that the steady state concentration of FadR is the same for all three architectures prior to switching to the ON-state. Likewise, in Figure 4B-C for fair comparison, *fadR* promoter strengths for both architectures were set to achieve same concentration of sequestered FadR in the ON-state (and thus equal recovery times).

Acknowledgements

This work was funded by the Human Frontier Science Program through a Young Investigator Grant awarded to F.Z. and D.O (grant no. RGY-0076-2015) and by the US National Science Foundation (MCB1453147) to F.Z.

Figures

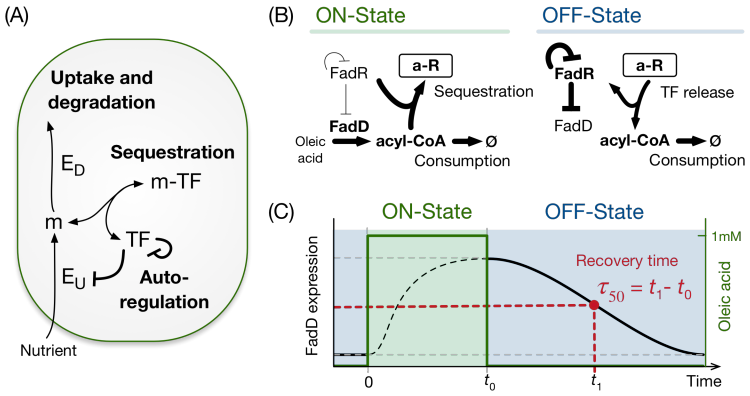

Figure 1. General architecture of a bacterial nutrient uptake system. (A) Regulation of nutrient uptake by a metabolite-responsive transcription factor (MRTF), a ubiquitously observed control system in bacteria (see Supplementary Information, Table S1). (B) We use the *Escherichia coli* fatty acid uptake as a model system. The ON-state is defined by induction at a constant level of oleic acid, which is imported as acyl-CoA by uptake enzyme FadD. Acyl-CoA sequesters the transcription factor FadR, which de-represses expression of the uptake enzyme. The OFF-state is defined by the wash out of oleic acid after some time t_0 in the ON-state. Release of sequestered FadR recovers its repression on FadD synthesis. FadR is also subject to negative autoregulation. (C) Schematic of the experiments and simulations in this work, with temporary induction by oleic acid (green line). To quantify the recovery of FadD levels in the OFF-state, we define the recovery time (τ_{50}) as the time it takes to drop to half way between maximum and minimum concentrations.

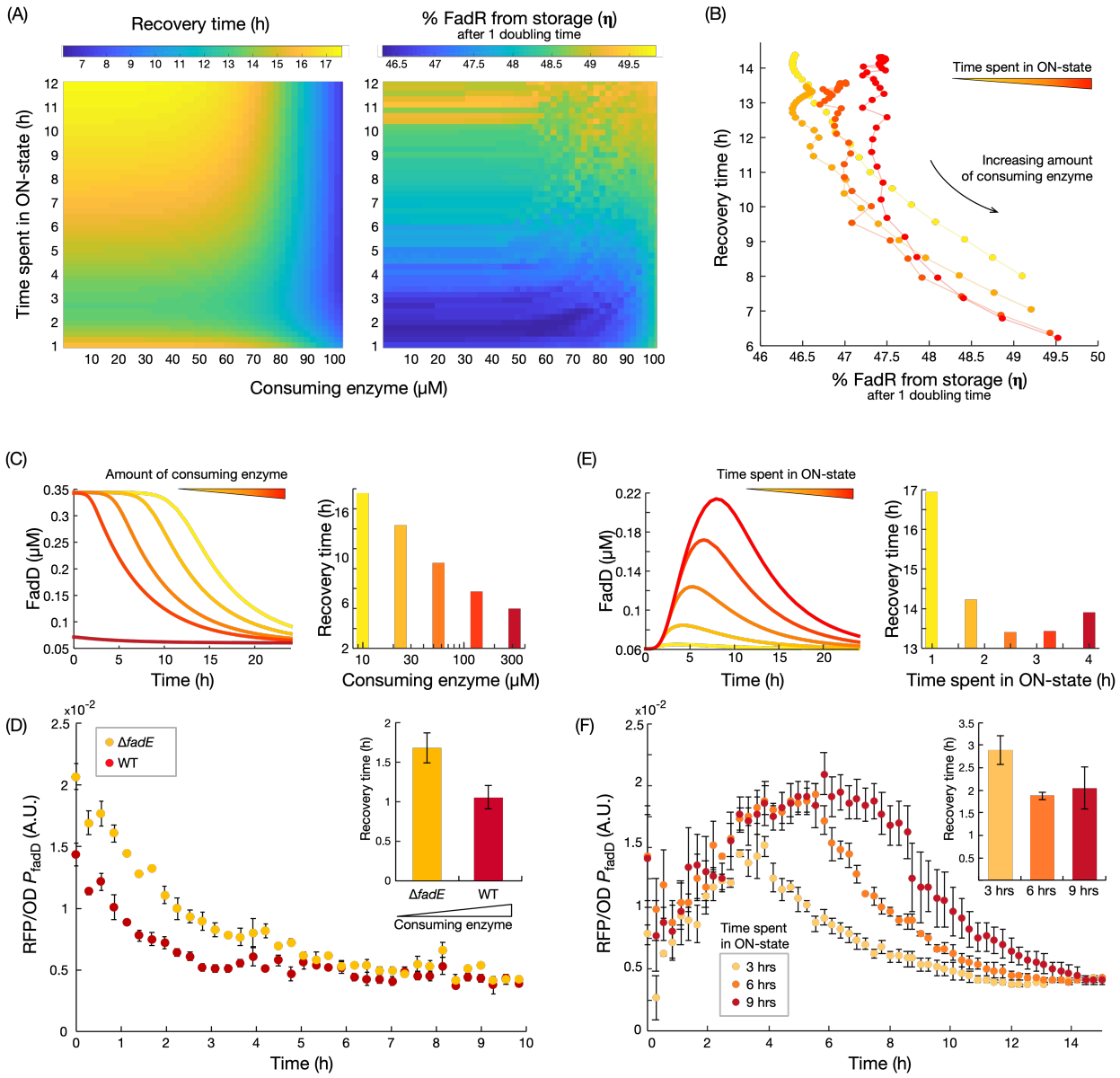

Figure 2. Speed of metabolite consumption in OFF-state and time spent in ON-state shape recovery time. (A) Predicted recovery time (τ_{50}) and proportion of free FadR released from sequestration after one doubling time (η) for variations in the amount of consuming enzyme and time spent in the ON-state. (B) Inverse relation between the proportion of released FadR (η) and predicted recovery time. (C) Simulated time course of FadD concentration in OFF-state and predicted recovery times for increasing concentration of acyl-CoA consuming enzyme. Model predicts shorter recovery times for enzyme abundance. (D) Measured time course of *fadD* expression when switching from ON- to OFF-state for strains with low (Δ*fadE*-reporter) and high (WT-reporter) concentration of acyl-CoA consuming enzyme. Strains were switched from M9G+1mM oleic acid to M9G media at time zero. Error bars represent standard error of the mean (SEM) from biological triplicates (n=3). Recovery times were calculated from exponential fits to each of the triplicate time course data (inset). Error bars represent SEM from biological

triplicates (n=3). (E) Time course simulations of FadD induction and recovery dynamics and predicted recovery times for variations increasing times spent in the ON-state. (F) Measured time course of *fadD* expression in WT-reporter grown in ON-state (M9G+1mM oleic acid) for 3, 6 and 9 hours, and then switched to OFF-state (M9G). Error bars represent SEM from biological triplicates (n=3). Recovery times were calculated from exponential fits to each of the triplicate data, based on all data points from the time of switch. Error bars represent SEM of fitted recovery times (n=3).

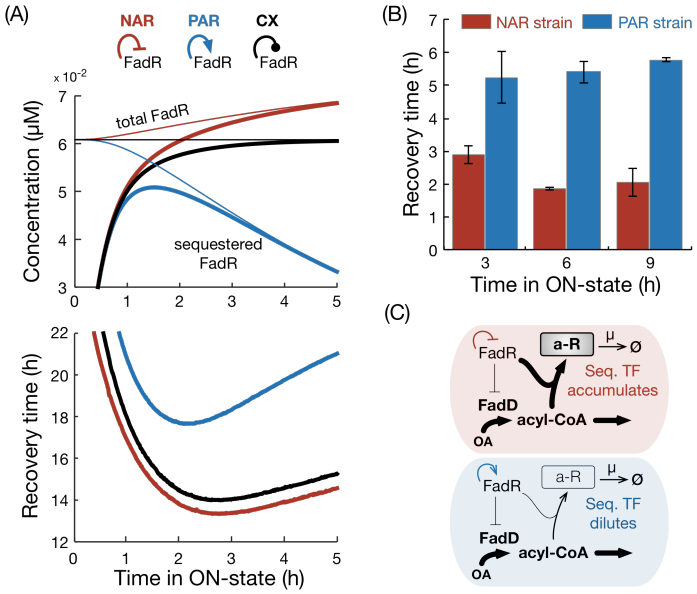

Figure 3. Impact of regulatory architecture on the recovery time after nutrient depletion. (A, top) Simulated steady state concentrations of sequestered (thick line) and total FadR (thin line) for varying times spent in the ON-state for three regulatory architectures of FadR; constitutive expression (black line) is represented by a blunt line. (A, bottom) Predicted recovery times for each architecture. (B) Measured recovery times in the WT (WT-reporter) and positively autoregulated strain (PA-reporter, Supplementary Table 6) for 3, 6 and 9 hours spent in ON-state. Recovery times were calculated from exponential fits to each of the triplicate time course data (data in Supplementary Information S8) and error bars represent SEM of the calculated values (n=3). (C) Schematics of negative and positive autoregulation affect the build-up of sequestered FadR in the ON-state.

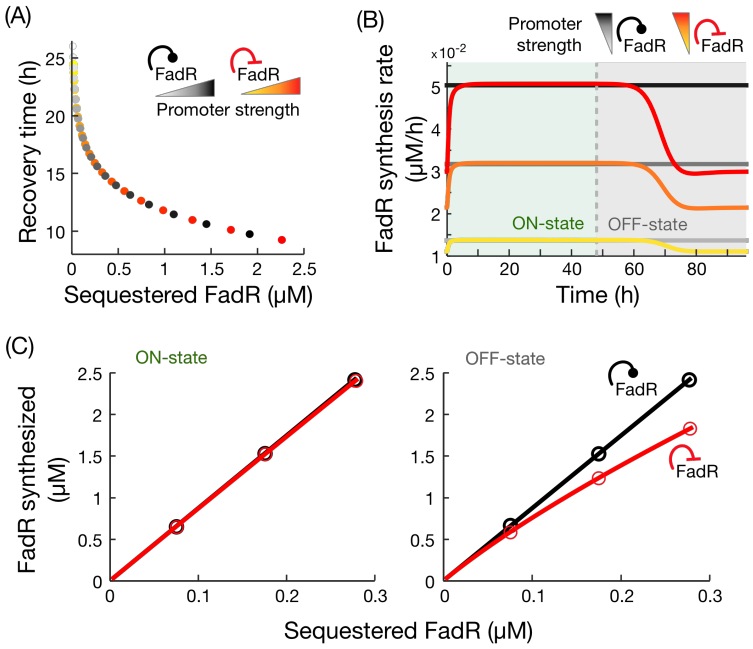

Figure 4. Comparison of recovery dynamics in constitutive expression and negative autoregulation. (A) Simulated recovery time for variations in the promoter strength; both architectures can achieve similar recovery times. (B) Time course simulations of FadR synthesis rates during ON-state (1mM oleic acid) and OFF-state, for increasing promoter strengths; yellow curve is for the promoter strength fitted from data (Table S3). (C) Cost of FadR synthesis for increasing concentrations of sequestered FadR, modified by changes to *fadR* promoter strength. Circles correspond to costs associated to simulations shown in (B). Details of simulations in Methods.